CdSe/CdS/ZnS and CdSe/ZnSe/ZnS Core−Shell−Shell Nanocrystals

Dmitri V. Talapin,*,†,‡ Ivo Mekis,† Stephan Götzinger,§ Andreas Kornowski,† Oliver Benson,§ and Horst Weller†

Institute of Physical Chemistry, University of Hamburg, Grindelallee 117, 20146 Hamburg, Germany, and Institut für Physik, Humboldt-Universität zu Berlin, Hausvogteiplatz 5-7, 10117 Berlin, Germany

Received: August 5, 2004; In Final Form: September 17, 2004

We report the synthesis and characterization of highly luminescent colloidal nanocrystals consisting of CdSe cores protected with double inorganic shells (core−shell−shell nanocrystals). The outer ZnS shell provides efficient confinement of electron and hole wave functions inside the nanocrystal as well as high photochemical stability. Introducing the middle shell (CdS or ZnSe) sandwiched between CdSe core and ZnS outer shell allows considerable reducing strain inside nanocrystals because CdS and ZnSe have the lattice parameter intermediate to those of CdSe and ZnS. In contrast to CdSe/ZnS core−shells, in the core−shell−shell nanocrystals ZnS shell grows nearly defect free. Due to high quality of the ZnS shell, the core−shell−shell nanocrystals exhibit PL efficiency and photostability exceeding those of CdSe/ZnS nanocrystals. Preferential growth of the middle CdS shell in one crystallographic direction allows engineering the shape and luminescence polarization of the core−shell−shell nanocrystals.

Introduction

Colloidal luminescent semiconductor nanocrystals attract considerable attention as potential candidates for LED's and displays,[1] photoluminescent and chemiluminescent biological labels,[2,3] etc. The advantages of semiconductor nanocrystals in comparison to the other emitting species (e.g., organic fluorescent dyes, rare-earth based phosphors, etc.) are the possibility of tuning the emission color by simply changing the nanocrystal size, excellent color purity, and the possibility of device fabrication by high-throughput solution based processes such as spin-coating and jet-printing.[1,4]

The key parameters that determine applicability of luminescent nanocrystals in the mentioned above applications are (i) high luminescence quantum efficiency, (ii) stability of luminescent properties under real operation conditions, and (iii) solubility of nanocrystals in a desired solvent. All these problems deal with the proper passivation of dangling bonds present on the nanocrystal surface. Attaching organic ligands to the nanocrystal surface can provide solubility to nanocrystals and, in certain cases, can allow high photoluminescence (PL) quantum efficiency.[5] However, the organic ligands are labile and in dynamic equilibrium with the surrounding medium. As a result, the luminescence efficiency is strongly dependent on the nanocrystal's surroundings and usually shows a tendency to drop in time due to oxidation of the particle surface.[6]

Growing a thin shell of a wide band gap semiconductor on the outside of the emitting nanocrystal allows substantial improvement of their stability. Such core−shell particles exhibit efficient luminescence with stability superior to single phase nanopaticles and organic dyes[2,7] and are of practical interest for biological imaging and light-emitting devices.

For the visible spectral range CdSe nanocrystals are considered as the most promising emitting material because their emission color can be precisely adjusted from blue to red. Several wide band gap semiconductors (ZnS,[8,9] CdS,[6,10−12] ZnSe[13,14]) were employed as the shell material. ZnS is a nontoxic, chemically stable wide band gap (3.8 eV for the bulk material) semiconductor. Potentially, the ZnS shell should provide the best passivation of CdSe core. However, the large mismatch (ca. 12%) between CdSe and ZnS lattice parameters induces the strain at the interface between the core and the shell. It has been shown that if the thickness of the ZnS shell exceeds ~2 monolayers, the interfacial strain leads to formation of misfit dislocations relaxing the nanocrystal structure.[8,15] The defects in the ZnS shell negatively affect both the PL efficiency and stability of CdSe/ZnS nanocrystals with thick shells. It is worth mentioning that the particle size distribution broadens substantially upon growing the ZnS shell around monodisperse CdSe cores.[8]

In the case of CdSe/CdS and CdSe/ZnSe core−shells, the lattice mismatch between the core and the shell materials is relatively small. In the case of CdSe/CdS nanocrystals the coherent epitaxial growth of the CdS shell has been reported.[11,12] As a result of the low concentration of defects in the shell, CdSe/CdS and CdSe/ZnSe nanocrystals exhibit very high PL quantum efficiencies, up to 80−90%.[6,10,13] However, the band gaps of CdS and ZnSe are not large enough to provide the potential barrier necessary to block both electrons and holes inside CdSe core.[8,12] Moreover, the CdS and ZnSe shells can be excited by UV light broadly used in biological tagging applications. The direct excitation of the nanocrystal shell causes its fast photooxidation that makes CdSe/CdS and CdSe/ZnSe nanocrystals unsuitable for many biolabeling applications.

We propose the general way of improving PL efficiency, stability, and robustness of luminescent nanocrystals. Our approach is based on engineering both energy band gap and lattice spacing inside a heterogeneous nanocrystal. We propose to introduce between the emitting core and the wide band gap

* Corresponding author. E-mail: talapin@chemie.uni-hamburg.de. Fax: +49-40-42838-3452. Homepage: http://www.chemie.uni-hamburg.de/pc/Weller/.

† University of Hamburg.

‡ Current address: IBM, T. J. Watson Research Center, 1101 Kitchawan Rd., Yorktown Heights, NY 10598.

§ Humboldt-Universität zu Berlin.

10.1021/jp046481g CCC: $27.50
Published on Web 11/12/2004

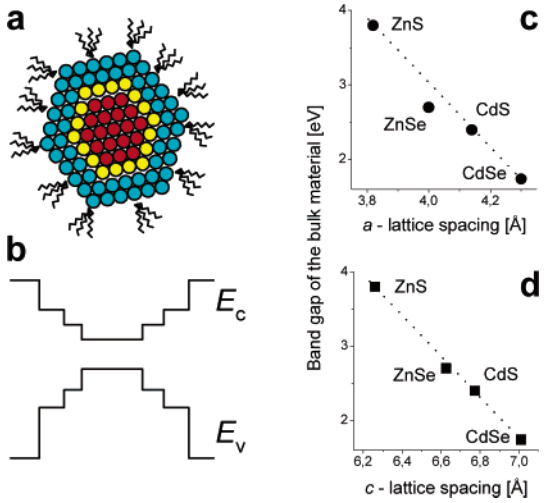

Figure 1. Core−shell−shell nanocrystal: (a) schematic outline and (b) the energy level diagram; (c, d) relationship between band gap energy and lattice parameter of bulk wurzite phase CdSe, ZnSe, CdS and ZnS.

shell a thin layer of a semiconductor with the lattice spacing intermediate to CdSe and ZnS (Figure 1). Such double shell (or core−shell−shell, CSS) structure allows a stepwise change of lattice spacing from the emitting CdSe core and the protecting ZnS shell. This design should allow considerable reducing of the strain inside nanocrystals. As materials for the middle shell we employ CdS and ZnSe. In bulk, these materials have both the band gap and the lattice spacing intermediate to CdSe and ZnS (Figure 1). Recently, Manna et al. reported the synthesis of the graded CdS/ZnS shells on colloidal CdSe nanorods.[16] However, to the best of our knowledge, no approaches to synthesis luminescent nanocrystals with distinct core−shell−shell structure with controllable thickness of both middle (CdS) and outer (ZnS) shells have been reported so far.

Experimental Section

Chemicals. All chemicals used were of analytical grade or of highest purity available. Toluene, methanol, *n*-hexane (all anhydrous, Aldrich), cadmium acetate ($Cd(Ac)_2$, 99.99%, ChemPur), selenium (99.999%, ChemPur), zinc acetate ($Zn(Ac)_2$ 99.99%, Aldrich), bis(trimethylsilyl)sulfide (Aldrich), diethyl zinc (1 M solution in hexane, Aldrich), *n*-octylphosphonic acid (OPA, 99%, Alfa Aesar), *n*-tetradecylphosphonic acid (TDPA, 99%, Alfa Aesar), and H_2S gas (1 L bottles, Messer Griesheim) were used as received. Dimethylcadmium (99.99%, EpiChem) was filtered through a 0.2 μm PTFE filter and stored at −35 °C in a glovebox. Tri-*n*-octylphosphine (further referred to as TOP, 90%, Fluka) was purified by distillation. Tri-*n*-octylphosphine oxide (TOPO, >98%, Merck or >90%, Alfa Aesar) and hexadecylamine (HDA, >92%, Merck) were purified and degassed in the reaction vessel by heating under vacuum for 1 h at temperatures slightly below their boiling points.

Apparatus. UV−vis absorption spectra were measured at room temperature with a Cary 50 UV−vis spectrometer (Varian). Photoluminescence (PL) spectra were measured at room temperature with a FluoroMax-2 spectrofluorometer (Instruments SA) on colloidal solutions having an optical density of less than 0.2 at the excitation wavelength (400 or 450 nm). PL quantum efficiency measurements were performed as described in ref 6. Single particle spectroscopy was carried out at room temperature in an epifluorescence microscope similar to previous descriptions.[17] Powder XRD measurements were performed on a Philips X'Pert PRO X-ray diffraction system. Samples for XRD measurements were prepared by dropping a colloidal suspension of nanocrystals in chloroform or hexane on a standard single crystal Si support and evaporating the solvent. High resolution transmission electron microscopy (HRTEM) and energy-dispersive X-ray analysis (EDX) were performed on a Philips CM-300 microscope operating at 300 kV. Samples for TEM investigations were prepared by dropping dilute solutions of properly washed nanocrystals in toluene or hexane onto 400-mesh carbon-coated copper grids allowing the solvent to immediately evaporate.

Synthesis of CdSe/CdS/ZnS and CdSe/ZnSe/ZnS Nanocrystals. Typical synthetic procedures for CdSe/CdS/ZnS and CdSe/ZnSe/ZnS nanocrystals are as follows. In the synthesis of *spherical CdSe/CdS/ZnS nanocrystals*, CdSe/CdS nanocrystals with ~3.2 nm CdSe core and ~1.2 nm thick CdS shell were prepared in the HDA−TOPO−TOP stabilizing mixture from $Cd(CH_3COOH)_2$, TOPSe and H_2S as described in ref 6 and isolated from crude solution inside a nitrogen-filled glovebox. A 25 mg sample of freshly prepared CdSe/CdS nanocrystals was dissolved in 6 g of TOPO and 4 g of HDA. To overcoat CdSe/CdS nanocrystals with a ZnS shell, this solution is heated to 210 °C and Zn:S stock solution is added dropwise. The Zn:S stock solution is prepared by mixing of 0.4 mL of 1 M solution of $Zn(C_2H_5)_2$ in hexane, 0.1 mL of bis(trimethylsilyl)sulfide and 3 mL of TOP. The thickness of the ZnS shell depends on the amount of the Zn:S stock solution added. After completing the ZnS shell growth, the reaction mixture is cooled to 90 °C and left at this temperature for 1 h. *CdSe/CdS/ZnS nanorods* are synthesized by growing a ZnS shell around CdSe/CdS nanorod heterostructures prepared as described in ref 12. The growing of the ZnS shell around CdSe/CdS nanorods should be performed at relatively low temperature (175−180 °C), and all other reaction conditions are similar to those used for the synthesis of spherical CdSe/CdS/ZnS nanocrystals. *CdSe/ZnSe/ZnS nanocrystals* are synthesized as follows: 30 mg of ~3.6 nm HDA−TOPO−TOP capped CdSe nanocrystals prepared as described in ref 18 are dissolved in 7 g of TOPO and 4.5 g of HDA, and the solution is heated to 190 °C. Growth of the ZnSe shell is induced by slow addition of Zn:Se precursors (0.3 mmol of $Zn(C_2H_5)_2$, 0.39 mmol of TOPSe dissolved in 3 mL TOP). The CdSe/ZnSe nanocrystals are isolated from crude solution by precipitating them with methanol inside a nitrogen-filled glovebox and redissolved in 10 g of TOPO and 6 g of HDA. The outer ZnS shell is grown at 200−220 °C by slow adding Zn:S stock solution prepared by mixing 1 mL of 1 M solution of $Zn(C_2H_5)_2$ in hexane, 0.46 mL of bis(trimethylsilyl) sulfide and 6 mL of TOP. All highly luminescent core−shell−shell nanocrystals can be isolated from crude solutions by precipitating them with ethanol and redispersed in chloroform. The "greener" recipes used in the synthesis of core, core−shell, and core−shell−shell nanocrystals are given in the Supporting Information.

Results and Discussion

Synthesis of Core−Shell−Shell Nanocrystals. Nearly monodisperse CdSe spherical nanocrystals are synthesized in a three-component stabilizing mixture containing hexadecylamine (HDA), trioctylphosphine oxide (TOPO), and trioctylphosphine (TOP), using either organometallic[18] or "greener" precursors.[6] For synthesis of both CdSe/CdS/ZnS and CdSe/ZnSe/ZnS nanocrystals we have adopted and modified the recipes previously employed for preparation of core−shell particles with a single-phase shell (CdSe/CdS,[6,10−12] CdSe/ZnSe,[13] CdS/ZnS,[19]

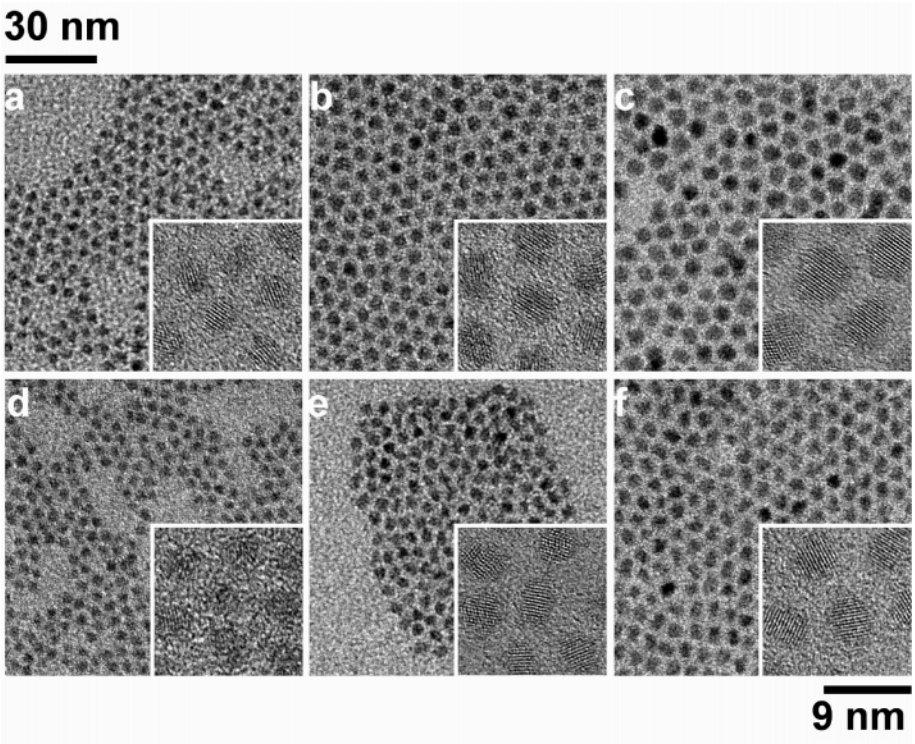

Figure 2. TEM and HRTEM images of (a) CdSe, (b) CdSe/CdS, and (c) CdSe/CdS/ZnS nanocrystals prepared by consecutive growing CdS and ZnS shells around the same CdSe cores. TEM and HRTEM images of (d) CdSe, (e) CdSe/ZnSe, and (f) CdSe/ZnSe/ZnS nanocrystals prepared by consecutive growing ZnSe and ZnS shells around the same CdSe cores.

CdSe/ZnS[8,9,12]). Generally, both organometallic and "greener" precursors allow preparation of CSS nanocrystals with nearly identical luminescent properties. The use of highly reactive dimethylcadmium and diethylzinc as the precursors for CdSe cores and a CdS/ZnS or ZnSe/ZnS shell is useful in the case of one-pot synthesis of CSS nanocrystals because these precursors allow achieving nearly quantitative reaction yields[6] and do not contaminate crude solutions with the reaction byproducts. It is worth mentioning that the organometallic and "greener" synthetic routes are compatible. For example, CdSe cores can be prepared from $Cd(CH_3COO)_2$ and TOPSe, capped with CdS shell by adding H_2S gas, whereas the outer ZnS shell can be grown using diethylzinc and bis(trimethylsilyl) sulfide as zinc and sulfur precursors, respectively. To be sure that our nanocrystals have the distinct core−shell−shell structure, we separated and purified nanocrystals before and after growing of the middle shell. To achieve good reproducibility in the synthesis of core−shell−shell nanocrystals, we paid special attention to optimization of each preparation stage. A narrow size distribution of both core and core−shell particles is strongly desirable to eliminate size-selection procedures.

Figure 2 shows representative TEM and HRTEM images of initial CdSe core, core−shell, and CSS nanocrystals. One can see the increase of mean nanocrystal size caused by growing the first (CdS or ZnSe) and the second (ZnS) shells. High-resolution TEM images (insets in Figure 2) of core, core−shell, and CSS nanocrystals show lattice planes that extend straight across the particles, with no evidence of an interface between the core and shells. This most likely implies that the growth of both middle (CdS or ZnSe) and outer ZnS shell occurs in the regime of coherent epitaxy.[8]

Particle Size Distribution. The width of size distribution of CSS nanocrystals remains narrow (<10%) even for the nanocrystals with thick (>5 monolayers) shells (Figures 4c,f). Both CdSe/CdS/ZnS and CdSe/ZnSe/ZnS nanocrystals reproducibly exhibit size distributions considerably narrower than those reported for CdSe/ZnS nanocrystals. The growth of ZnS shell on CdSe cores is accompanied by significant broadening of particle size distribution.[8] To understand this difference in the behavior of CdSe/ZnS and CSS nanocrystals, we should discuss the parameters affecting size distribution of colloidal nanoparticles. To grow the shell, the molecular precursors (further referred to as "monomers") are slowly added into a colloidal solution of core nanocrystals. The kinetics of shell growth can be limited either by diffusion of monomers toward the nanocrystal surface or by the rate of decomposition of monomers on the nanocrystal surface. Theoretical considerations predict that diffusion-limited growth should always result in narrowing of the particle size distribution.[20,21] Such narrowing or "focusing" of the size distribution induced by addition of monomers was observed experimentally in the synthesis of single phase nanocrystals (CdSe,[22] CdTe[23]). The broadening of the size distribution observed in the synthesis of CdSe/ZnS core−shell nanocrystals[8] can be considered as evidence of reaction-controlled kinetics of shell growth. The lattice mismatch between the core and the shell creates a barrier for nucleation of the shell material. Moreover, the interfacial strain at the core−shell interface gives an additional contribution to the chemical potential of the whole nanocrystal. Note that this strain-induced contribution depends on the presence of defects and dislocations inside the shell, which may vary from particle to particle. These arguments may explain why the presence of a highly strained interface inside a nanocrystal causes poor control over kinetics of shell growth which, in turn, result in broadening of the particle size distribution. Reducing the interfacial strain by engineering the lattice spacing (e.g., introducing the middle shell) seems to be the general way to achieving narrow in situ size distributions of heterogeneous nanocrystals (Figure 2).

Shape Engineering. In addition to reducing the interfacial strain between the core and the outer shell, the middle shell in

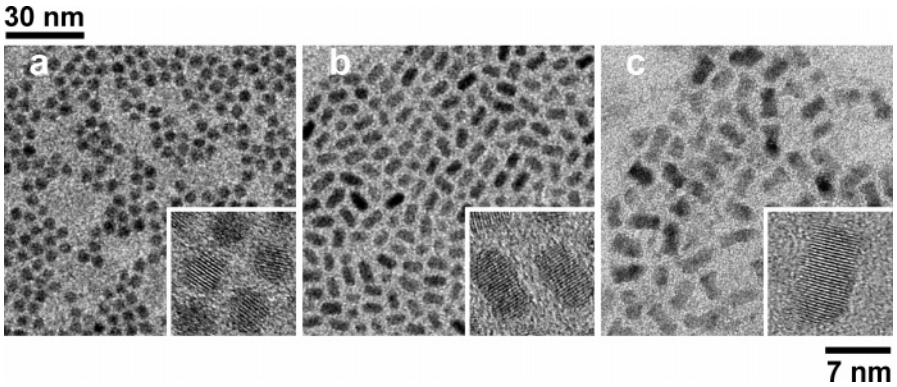

Figure 3. TEM and HRTEM images of (a) spherical CdSe cores, (b) CdSe/CdS heterostructure nanorods prepared by growing CdS shell selectively on the $\{00\bar{1}\}$ facet of the CdSe cores, and (c) CdSe/CdS/ZnS nanorods prepared by uniform coating of CdSe/CdS nanorods by ZnS shell.

the CSS nanocrystal can also determine the particle shape. Recently, we have demonstrated the possibility of synthesizing colloidal heterostructure nanorods consisting of spherical CdSe core and CdS rodlike shells grown preferentially on the $\{00\bar{1}\}$ facet of the CdSe core[12] (Figure 3a,b). The passivation of the spherical CdSe core with the elongated CdS shell results in efficient band gap photoluminescence (PL) with PL quantum efficiencies up to 75%. The electronic structure of CdSe/CdS nanorods provides a very different level of confinement for electrons and holes. The hole is strongly confined to the CdSe core and maintains 0-D character, whereas the electron gains 1-D character due to delocalization into the 1-D rodlike shell. This quantum confinement regime results in linear polarization of PL along the nanorod.[12,24] The CdSe/CdS nanorod heterostrucrure can be uniformly coated with ZnS shell, as shown in Figure 3c. Growing of ZnS shell allows obtaining robust colloidal nanoparticles with efficient and stable linearly polarized luminescence, which is very attractive for tagging and light-emitting applications. The asymmetric shape of the CdSe/CdS/ZnS nanocrystals allows their easy unidirectional aligning, e.g., in the stretched polymer films.[12]

Powder X-ray Diffraction. The information about nanocrystal morphology and the mechanism of shell growth can be obtained by comparison of the powder-XRD patterns of core and core/shell nanocrystals. In the case of CdSe/ZnS core−shell nanocrystals, several regimes of the shell growth were observed depending on the ZnS shell thickness. The shell thinner than ∼2 monolayers grows preferentially by coherent epitaxy.[8] Previous XRD and Raman studies indicate the transition from the coherent to incoherent epitaxial growth of the shell which occurs at ZnS coverage of ∼2 monolayers.[8] The shell thicker than ∼ 2 monolayers grows with the lattice parameter of bulk ZnS.[8,15] This implies that at certain coverage there is a threshold for inducing dislocations.

Powder-XRD patterns of nearly spherical CdSe/ZnSe/ZnS and rodlike CdSe/CdS/ZnS nanocrystals are shown in Figure 4. The evolution of the powder X-ray diffraction patterns during the growing of the shells around spherical CdSe particles shows that the wurtzite phase of CdSe cores carries through to the shells. The higher intensity and the smaller width of the (002) reflection in Figure 4, right panel shows that the long axis of the CdSe/CdS and CdSe/CdS/ZnS nanorods is identical with the *c*-axis of the wurtzite structure. The attenuation of the (102) and (103) reflexes in the powder X-ray diffraction patterns can be explained by the presence of zinc blende stacking faults along the (002) direction that is very typical for wurtzite II−VI nanocrystals.[8,25] In both CdSe/ZnSe/ZnS and CdSe/CdS/ZnS nanocrystals the positions of (110) and (112) reflections from

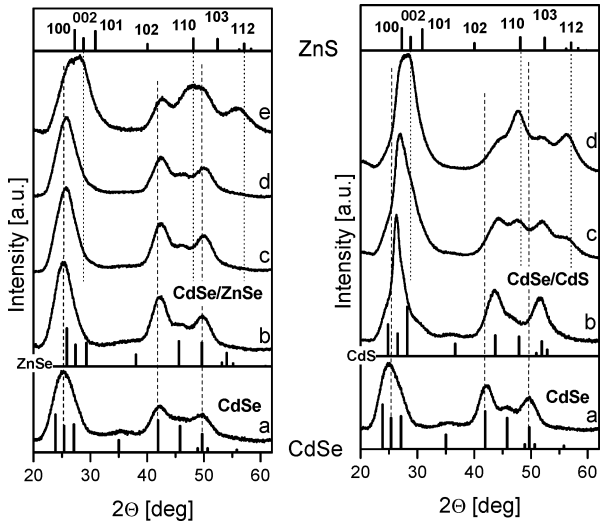

Figure 4. Left: powder X-ray (Cu Kα radiation) diffraction patterns of (a) 3.5 nm spherical CdSe cores, (b) CdSe/ZnSe core−shells (thickness of ZnSe shell ∼1.4 monolayers), (c, d, e) CdSe/ZnSe/ZnS nanocrystals with the thickness of ZnS shell ∼1 monolayer (c), ∼2 monolayers (d), and ∼4 monolayers (e). Right: powder XRD patterns of (a) 4.0 nm spherical CdSe cores, (b) CdSe/CdS nanorods (aspect ratio ∼2.8:1), and (c, d) CdSe/CdS/ZnS nanorods with thin ∼2 monolayer (c) and thick ∼3.5 monolayer (d) ZnS shells. The higher intensity and smaller width of the (002) reflection shows that the long axis of the CdSe/CdS nanorods is the *c*-axis of a wurtzite structure. The bulk wurtzite CdSe, CdS, ZnSe, and ZnS references are given as line patterns.

the ZnS shell are shifted toward smaller 2θ angles, which corresponds to the expansion of ZnS lattice by ∼3% (Figure 4). At the same time, the CdSe core reflections are shifted toward larger 2θ angles reflecting the compression of lattice plains of CdSe core by at least 2%. The contraction of CdSe core lattice together with the expansion of ZnS lattice provide the evidence that the structure of the CSS nanocrystal does not relax the interfacial strain by introducing misfit dislocations in outer ZnS shell. The middle "wetting" layer of CdS or ZnSe provides a smooth cascade-like transition between CdSe and ZnS lattices. As a consequence, we may expect a lower concentration of crystalline defects in the ZnS shell, which is in agreement with HRTEM investigations (Figures 2 and 3).

Optical Properties. Figure 5a shows UV−vis and PL spectra of CdSe, CdSe/ZnSe, and CdSe/ZnSe/ZnS nanocrystals with the same size of CdSe core. The formation of a ZnSe shell around CdSe cores results in a drastic improvement of PL quantum efficiency (up to 70−85%) accompanied by the red shift of both the first absorption maximum and PL band. The observed red shift shows that ZnSe shell cannot provide potential

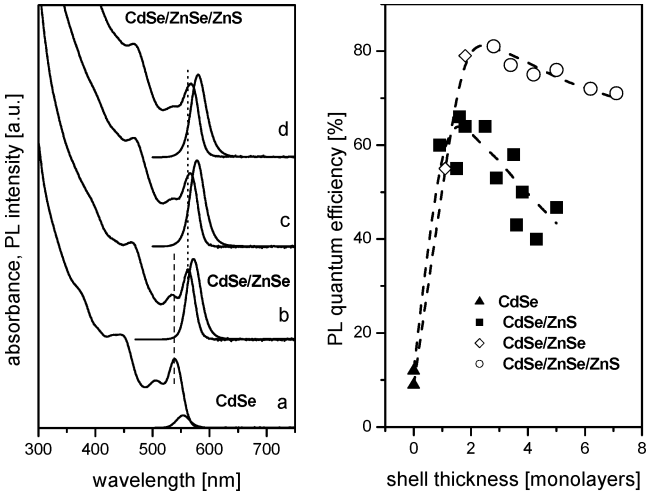

Figure 5. Left: absorption and PL spectra of (a) CdSe cores, (b) CdSe/ZnSe core−shells (thickness of ZnSe shell ∼2 monolayers), (c, d) CdSe/ZnSe/ZnS nanocrystals with the thickness of ZnS shell ∼2 monolayers (c) and ∼4 monolayers (d). Right: room-temperature PL quantum yields of CdSe, CdSe/ZnSe, and CdSe/ZnSe/ZnS nanocrystals dissolved in chloroform. For comparison, the dependence of PL quantum yield on the shell thickness for various samples of CdSe/ZnS nanocrystals is shown.

barriers large enough to prevent the leakage of the exciton into the shell. Growing the shell of ZnS around CdSe/ZnSe nanocrystals results in a small (∼15 meV) red shift of absorption and PL spectra. The PL quantum efficiency of CdSe/ZnSe/ZnS nanocrystals is nearly as high as that of CdSe/ZnSe. It is a well-known fact that PL efficiency of CdSe/ZnS nanocrystals shows the extremal dependency on the thickness of ZnS shell.[8,19] An increase of the ZnS shell thickness above 2−3 monolayers is accompanied with the decrease in the PL quantum efficiency (Figure 5b). This effect has been attributed to the changes in morphology of the ZnS shell discussed above. Most probably, the dislocations and grain boundaries inside the ZnS shell introduced upon the transition from coherent to incoherent shell growth play the role of nonradiative recombination sites.

In the case of CdSe/ZnSe/ZnS nanocrystals the effect of a decreasing PL efficiency with increasing shell thickness is much less pronounced (Figure 5b). Moreover, we have observed for CSS nanocrystals much better reproducibility of the PL quantum yield whereas in the case of CdSe/ZnS this parameter can significantly vary from run to run (Figure 5b). The maximum of PL efficiency is approached after growing a ∼2 monolayer thick ZnSe shell. We attribute the difference in behavior of CdSe/ZnS and CdSe/ZnSe/ZnS nanocrystals to the better crystallinity of the shell in the latter case. CdSe/CdS/ZnS nanocrystals with both spherical and rodlike shape exhibit luminescent properties similar to those of CdSe/ZnSe/ZnS nanocrystals. Summarizing results of many experiments allowed us to conclude that CdSe/ZnSe/ZnS nanocrystals exhibit slightly higher (by 5−10%) PL efficiency than CdSe/CdS/ZnS nanocrystals and nanorods.

Photochemical Stability. Long-term stability of nanocrystal luminescence is one of the key problems for the application of luminescent nanocrystals in commercial light-emitting devices. The core−shell nanocrystals show significant enhancement of photochemical stability as compared to bare cores. However, our experiments show that under UV illumination both CdSe/CdS and CdSe/ZnSe nanocrystals cannot compete in photostability with CdSe/ZnS ones (see, e.g., ref 6). The high stability of CdSe/ZnS nanocrystal determines their broad use for biological labeling and imaging.[2,26] To the best of our knowledge,

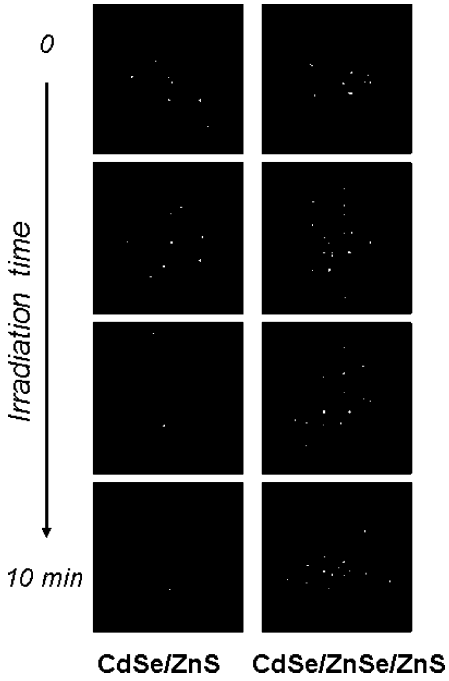

Figure 6. Single particle luminescence images of CdSe/ZnS (left column) and CdSe/ZnSe/ZnS (right column) nanocrystals excited by intense laser beam (514 nm) in air. The excitation intensity was chosen high enough to irreversibly bleach both nanocrystal samples on a short time scale. Each image is averaged over 10 s.

CdSe/ZnS nanocrystals are considered as the photochemically most stable colloidal luminescent semiconductor nanoparticles. We have compared the photochemical stability of CdSe/ZnS and CdSe/ZnSe/ZnS nanocrystals capped with the same combination of organic ligands (HDA, TOPO, and TOP). The size of the CdSe core was the same for both samples as well as the absorption cross-section at the excitation wavelength. The thickness of the shell was ∼4 monolayers in the case of CdSe/ZnS nanocrystals and ∼1.5 (ZnSe) plus ∼3 (ZnS) in the case of CdSe/ZnSe/ZnS nanocrystals. These values are optimal for both samples. We have found that CdSe/ZnS nanocrystals with relatively thin (2−4 monolayers) ZnS shell show better photostability than those with thicker shells. The colloidal solutions of both CdSe/ZnS and CdSe/ZnSe/ZnS nanocrystals exhibit highly stable luminescence. For example, the samples placed in front of the lamp with 36 W output power at 366 nm for more than 2 weeks does not show any significant change of their PL quantum efficiency (Figure S1, Supporting Information). To accelerate the nanocrystal photooxidation and gain direct insight to stability of individual nanocrystals, we deposited CdSe/ZnS and CdSe/ZnSe/ZnS nanocrystals on glass slides from very diluted colloidal solutions and irradiated them with intense laser beam (514 nm) in air. The time evolution of single-particle luminescence images clearly shows that CdSe/ZnSe/ZnS nanocrystals are considerably more stable than CdSe/ZnS ones under intense irradiation (Figure 6). The higher stability of CSS nanocrystals is the additional manifestation of improved crystallinity of outer ZnS shell. The dislocations and grain boundaries present in ZnS shell of CdSe/ZnS nanocrystals facilitate diffusion of oxygen to the CdSe core, which can be responsible for their faster photodegradation. It is worth mentioning that the effect of oxygen on the fluorescence efficiency and stability of single core−shell nanocrystals is not fully understood yet. Recently, we reported a dramatic enhancement of the fluorescence intensity from single CdSe/ZnS nanocrystals upon sudden

exposure to air from an evacuated surrounding.[27] Blinking statistics of fluorescence of core−shell−shell nanocrystals can be substantially different in air and under anaerobic conditions. The comparison of photodegradation rate of single core−shell as well as core−shell−shell nanocrystals under different atmospheres can clarify the mechanism of photodegradation of luminescent nanocrystals.

Summary

Summarizing, we have developed the synthesis of novel type of luminescent semiconductor nanocrystals consisting of CdSe core and ZnS outer shell separated by either a CdS or a ZnSe layer to reduce strain at the interface between the core and outer shell. The comparison of CdSe/CdS/ZnS and CdSe/ZnSe/ZnS nanocrystals with CdSe/ZnS particles shows that introducing a wetting layer between the core and ZnS shell results in (i) a significant improvement of the outer ZnS shell crystallinity, (ii) more narrow particle size distributions upon ZnS shell growth, and (iii) control of the particle shape by asymmetrically growing CdS shell on CdSe cores. The better control of the shell quality provides the nanocrystals with more efficient and more stable luminescence. Among the other advantages of CSS nanocrystals in comparison with conventional core−shells, we mention their potentially lower toxicity in biological applications due to better protection of surrounding medium from the toxic elements present in the emitting CdSe core by nontoxic ZnS shell.

Acknowledgment. We thank Sylvia Bartholdi-Nawrath for assistance with TEM and HRTEM investigations, Felix Müller and Andrea Mazzei for help in the single particle spectroscopy measurements, and C. B. Murray for helpful discussions. This work was supported by the Deutsche Forschungsgemeinschaft through SFB 508 and SPP1113, and by NATO Scientific and Environmental Affairs Division.

Supporting Information Available: "Greener" synthetic recipes for CdSe, CdSe/CdS, CdSe/ZnSe, CdSe/CdS/ZnS, and CdSe/ZnSe/ZnS nanocrystals. Photodegradation of CdSe, CdSe/CdS, and CdSe/CdS/ZnS nanocrystals in colloidal solutions under the same illumination conditions (Figure S1). This material is available free of charge via the Internet at http://pubs.acs.org.

References and Notes

(1) Coe, S.; Woo, W.-K.: Bawendi, M. G.; Bulovic, V. *Nature* **2002**, *420*, 800.
(2) Bruchez, M. P.; Moronne, M.; Gin, P.; Weiss, S.; Alivisatos, A. P. *Science* **1998**, *281*, 2013.
(3) Poznyak, S. K.; Talapin, D. V.; Shevchenko, E. V.; Weller H. *Nano Lett.* **2004**, *3*, 693.
(4) Ridley, B. A.; Nivi, B.; Jacobson, J. M. *Science* **1999**, *286*, 746.
(5) Qu, L.; Peng, X. *J. Am. Chem. Soc.* **2002**, *124*, 2049.
(6) Mekis, I.; Talapin, D. V.; Kornowski, A.; Haase, M.; Weller, H. *J. Phys. Chem. B* **2003**, *107*, 7454.
(7) Chan, W. C. W.; Nie, S. *Science* **1998**, *281*, 2016.
(8) Dabbousi, B. O.; Rodriguez-Viejo, J.; Mikulec, F. V.; Heine, J. R.; Mattoussi, H.; Ober, R.; Jensen, K. F.; Bawendi, M. *J. Phys. Chem. B* **1997**, *101*, 9463.
(9) Hines, M. A.; Guyot-Sionnest, P. *J. Phys. Chem.* **1996**, *100*, 468.
(10) Peng, X.; Schlamp, M. C.; Kadavanich, A.; Alivisatos, A. P. *J. Am. Chem. Soc.* **1997**, *119*, 7019.
(11) Li, J. J.; Wang, Y. A.; Guo, W.; Keay, J. C.; Mishima, T. D.; Johnson, M. B.; Peng, X. *J. Am. Chem. Soc.* **2003**, *125*, 12567.
(12) Talapin, D. V.; Koeppe, R.; Götzinger, S.; Kornowski, A.; Lupton, J. M.; Rogach, A. L.; Benson, O.; Feldmann, J.; Weller H. *Nano Lett.* **2003**, *3*, 1677.
(13) Reiss, P.; Bleuse, J.; Pron, A. *Nano Lett.* **2002**, *2*, 781.
(14) Reiss, P.; Carayon, S.; Bleuse, J.; Pron, A. *Synth. Met.* **2003**, *139*, 649.
(15) Baranov, A. V.; Rakovich, Yu. P.; Donegan, J. F.; Perova, T. S.; Moore, R. A.; Talapin, D. V.; Rogach, A. L.; Masumoto, Y.; Nabiev, I. *Phys. Rev. B* **2003**, *68*, 165306.
(16) Manna, L.; Scher, E. C.; Li, L.-S.; Alivisatos, A. P. *J. Am. Chem. Soc.* **2002**, *124*, 7136.
(17) Empedocles, S. A.; Norris, D. J.; Bawendi, M. G. *Phys. Rev. Lett.* **1996**, *77*, 3873.
(18) Talapin, D. V.; Rogach, A. L.; Kornowski, A.; Haase, M.; Weller, H. *Nano Lett.* **2001**, *1*, 207.
(19) Steckel, J. S.; Zimmer, J. P.; Coe-Sullivan, S.; Stott, N. E.; Bulovic, V.; Bawendi, M. G. *Angew. Chem., Int. Ed.* **2004**, *43*, 2154.
(20) Talapin, D. V.; Rogach, A. L.; Haase, M.; Weller, H. *J. Phys. Chem. B* **2001**, *105*, 12278.
(21) Rogach, A. L.; Talapin, D. V.; Shevchenko, E. V.; Kornowski, A.; Haase, M.; Weller, H. *Adv. Funct. Mater.* **2002**, *12*, 653.
(22) Peng, X.; Wickham, J.; Alivisatos, A. P. *J. Am. Chem. Soc.* **1998**, *120*, 5343.
(23) Talapin, D. V.; Rogach, A. L.; Shevchenko, E. V.; Kornowski, A.; Haase, M.; Weller H. *J. Am. Chem. Soc.* **2002**, *124*, 5782.
(24) Müller, J.; Lupton, J. M.; Rogach, A. L.; Feldmann, J.; Talapin, D. V.; Weller, H. *Phys. Rev. Lett.* **2004**, *93*, 167402.
(25) Murray, C. B.; Norris, D. J.; Bawendi, M. G. *J. Am. Chem. Soc.* **1993**, *115*, 8706.
(26) Dubertret, B.; Skourides, P.; Norris, D. J.; Noireaux, V.; Brivanlou, A. H.; Libchaber, A. *Science* **2002**, *298*, 1759.
(27) Müller, J.; Lupton, J. M.; Rogach, A. L.; Feldmann J.; Talapin, D. V.; Weller, H. *Appl. Phys. Lett.* **2004**, *85*, 381.